Available online at www.sciencedirect.com

ScienceDirect

Ceramics International 40 (2014) 317–321

CERAMICS INTERNATIONAL

www.elsevier.com/locate/ceramint

A study on the precursor of vanadium pentoxide by the hydrothermal method

Jinxing Wang*, Weijie Yu, Shun Xu, Songyan Dai, Jiadong Wang, Chenxi Wang, Wen Zeng, Peishan Cao

College of Materials Science and Engineering, Chongqing University, Chongqing 400044, China

Received 20 March 2013; received in revised form 9 May 2013; accepted 1 June 2013
Available online 7 June 2013

Abstract

Different morphologies including bulk, layer by layer structure and nanosheets-like spheres of vanadium pentoxide (V_2O_5) precursor have been synthesized via a simple and direct hydrothermal method. Field emission scanning electron microscopy, X-ray powder diffraction and UV–vis diffuse reflectance were used to characterize the fabricated materials. The results showed that the reaction time had a great influence on the morphology evolution processes of the as-synthesized precursors. The photocatalysis measurements showed that the nanosheet-like spheres exhibited the highest activity for degrading rhodamine B under UV light. The possible morphology transformation mechanism and the schematic representation of the precursor are also discussed.

Keywords: Morphology transformation; Precursor; Hydrothermal; Formation mechanism; Photocatalysis

1. Introduction

Nanomaterials, which are often superior to their corresponding bulk materials [1–4], have attracted much attention due to their crucial roles in future technological applications. It is well known that the properties of materials such as physical, optical and electronic ones are greatly dependent on their shapes when their sizes were reduced to micrometer or nanometer scale [5]. So, many efforts have been devoted to the synthesis of materials with different shapes and sizes. To achieve the desired shapes and sizes, some surfactants, including different organic or inorganic oxidants and reductants, were effectively used. For instance, different inorganic salts, such as KNO_3, $Ca(NO_3)_2$, $La(NO_3)_3$, etc. were used to synthesize molybdenum trioxide nanobelts and prism-like particles. All these inorganic salts were added to control the morphologies of the final products [6]. Thiol, cetyltrimethyl ammonium bromide (CTAB), polyvinylpyrrolidone, $C_{12}H_{25}SO_3Na$ and H_2S, strontium nitrate and sodium tungstatsodium poly (4-styrenesulfonate) were used to obtain MoO_3 SWCNTs (single-walled carbon nanotubes) [7], V_2O_5 nanorod and nanoparticles [8], ZnO nanocrystals, ZnS nanomaterials [9–11] and hollow nanospheres and microspheres structure of tungsten trioxide [12], respectively.

Among the transition metal oxides, vanadium pentoxide (V_2O_5) has attracted great attention due to its good property for application on lithium-ion batteries [13] and photocatalysis [14,15]. In order to obtain vanadium pentoxide nanomaterial, different surfactants such as $KBrO_3$ [16], hydrogen peroxide (H_2O_2) [17], polyethyleneglycol (PEG) [18] and polyvinylpyrrolidone (PVP) [19] were used. Except for these surfactants mentioned above, oxalic acid is also a feasible and facile surfactant to prepare V_2O_5 in hydrothermal condition with the final process of calcination. While even using the same surfactant of oxalic acid as the reductant, different morphologies of vanadium pentoxide precursor were obtained during the preparation of V_2O_5 nanostructure, such as vanadium oxide microspheres [20–22], similar roselike nanostructures and nanorods [23]. However, the morphology mechanism and the morphology transformation process of vanadium pentoxide precursor have been rarely reported. In this work, we used the

*Corresponding author. Tel.: +86 23 6510 2466.
E-mail address: wjx@cqu.edu.cn (J. Wang).

0272-8842/$ - see front matter
http://dx.doi.org/10.1016/j.ceramint.2013.06.004

facile and controllable hydrothermal method to prepare the precursor of vanadium pentoxide, and observed the morphology transformation processes of the vanadium pentoxide precursor by increasing the reaction time without the change of the other parameters. In addition, the morphology transformation mechanism was discussed.

2. Experimental

2.1. Synthesis

Comparative experiments in the different reaction times with the other experimental parameters unchanged were carried out to approach different precursor morphologies of V_2O_5 via the hydrothermal method in a Teflon-lined autoclave. Four experimental programs were designed, which are named S1, S2, S3 and S4. Their detailed processes are as follows:

0.002 mol of ammonium metavanadate ($NH_4 \cdot VO_3$) was dissolved in 50 ml ethanol solution containing 0.02 mol of oxalic acid. After vigrous stirring for 2 h until the solution turned to brick-red suspension, it was transferred to a 25 ml stainless steel Teflon lined autoclave maintained at 180 °C for different reaction times. Later on, the obtained blue precipitates were collected and washed with deionized water and anhydrous ethanol for several times and then dried at 60 °C in air for 10 h. The precipitates which were maintained for 4 h, 8 h, 12 h and 24 h are named S1, S2, S3 and S4, respectively.

2.2. Measurements

The structure and morphology of the precipitates were characterized by X-ray diffraction (XRD) and field emission scanning electron microscopy (FESEM). A Rigaku D/Max-1200X diffractometry with the Cu Kα radiation operated at 30 kV and 100 mA was employed for the structure analysis. A Hitachi S-4300 SEM was operated for the surface morphologies observation. Diffuse reflectance UV–vis absorption spectra were obtained using a XPA photocatalytic reactor.

2.3. Photocatalytic activity

The photocatalytic performance of different morphologies of the precursors were evaluated via degradation of rhodamine B (RhB) under the irradiation of UV light. A 300 W Hg lamp was used as the UV source. The lamp was placed beside the RhB solution with a distance of 10 cm. In a typical protocol, 0.01 g catalyst was added to 100 ml of 1.0×10^{-5} M RhB dye solution. After that, the mixture was magnetically stirred in the dark for 30 min to establish an adsorption/desorption equilibrium and a 4 ml suspension was centrifuged to get clear RhB solution as a primary sample and then the mixture was exposed to UV light at room temperature. A 4 ml suspension was centrifuged to remove the catalysts every 20 min. The clear RhB solution was analyzed by UV–vis spectra with a Shimadzu UV-spectrophotometer 2100.

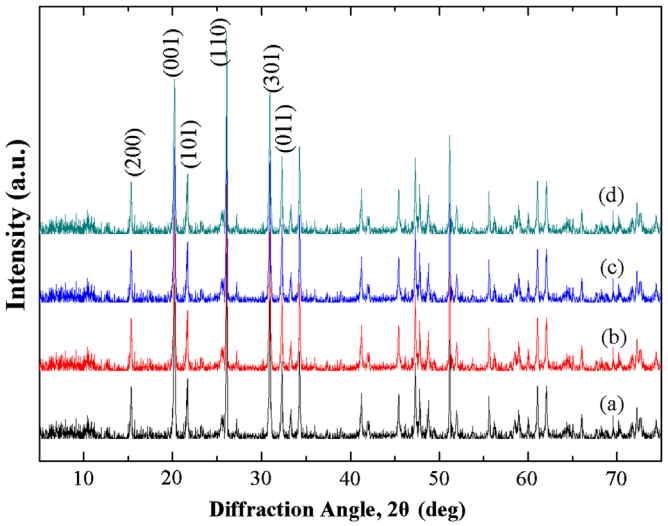

Fig. 1. XRD results of the four precipitates after calcined under 450 °C for 1 h at (a) S1 program (suspension liquid react at 180 °C for 4 h), (b) S2 program (suspension liquid react at 180 °C for 8 h), (c) S3 program (suspension liquid react at 180 °C for 12 h), (d) S4 program (suspension liquid react at 180 °C for 24 h).

3. Structural characterization and mechanism analysis

3.1. XRD analysis

Fig. 1 shows the XRD results of the calcined precipitates. The main diffraction peaks of 15.32°, 20.26°, 21.71°, 26.12°, 31.01° and 32.36° correspond to the characteristic diffraction of the (200), (001), (101), (110), (301) and (011) planes of the vanadium pentoxide, respectively. The diffraction peaks match well with those of the standard V_2O_5 pattern (PDF No. 65-0131). These XRD results demonstrating that the precipitates of four experimental programs were pure V_2O_5 powder.

3.2. SEM analysis

The morphology and structure of the samples were further investigated by FESEM. By increasing the reaction time with the other conditions unchanged, we successfully observed the morphology transformation process of vanadium pentoxide precursor, which are shown in Fig. 2. The results obtained from different reaction times are given on the left side in Fig. 2 and the corresponding magnified images of these results are given on the right side in Fig. 2, respectively. When the reaction time is 4 h, the morphology of the precursor powder is a bulk with edges and corners as shown in Fig. 2(a). The size of this bulk powder is more than dozens of micrometers. High resolution SEM observation reveals that the edges of the bulk are stacked by layers, which is marked by the yellow arrow (the right image in Fig. 2a). Fig. 2(b) is the morphology of the product which is obtained at 180 °C for 8 h. It is clearly seen that the primary bulk marked by the yellow arrow in the right image splits apart into many layers and some top layers start to bend. The thicknesses of the layers are about 30 nm and the split behavior starts at the end of the bulk. Then the

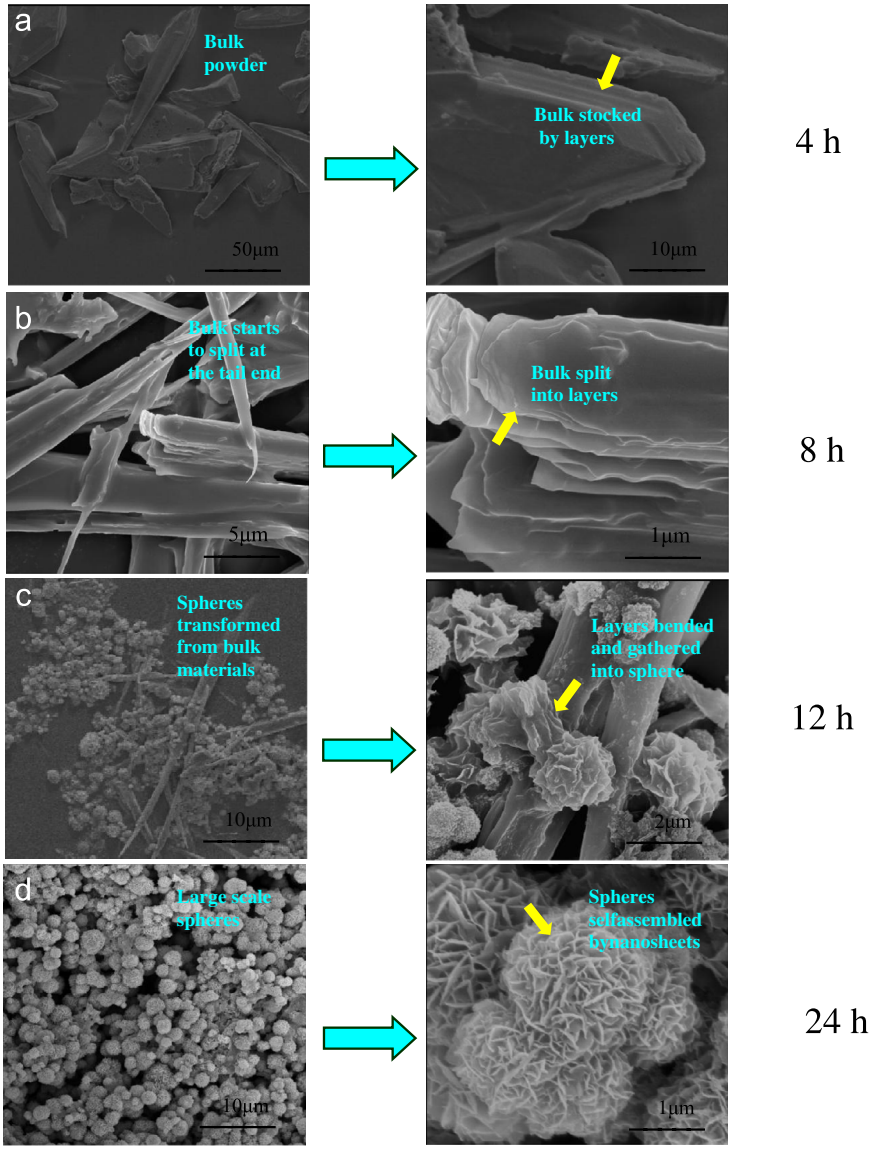

Fig. 2. Four different morphologies of vanadium pentoxide precursor nanostructures obtained at (a) S1 program (suspension liquid react at 180 °C for 4 h), (b) S2 program (suspension liquid react at 180 °C for 8 h), (c) S3 program (suspension liquid react at 180 °C for 12 h), (d) S4 program (suspension liquid react at 180 °C for 24 h). (For interpretation of the references to color in this figure , the reader is referred to the web version of this article.)

reaction time increase to 12 h and the SEM image of the product morphology is named (c). From the SEM image, we can clearly see the formation of some spheres on the bulk powder. The magnified image (the right image in Fig. 2c) shows that the spheres, which is evolution of the primary bulk powder, are assembled by many nanosheets. The average diameter of the nanosheet-like sphere is about 2 μm and the thickness of the nanosheet is about 30 nm. To investigate the final morphology of the vanadium pentoxide precursor, the reaction time was increased from 12 h to 24 h. The SEM image of the product obtained by hydrothermal treatment for 24 h is named (d). The image shows that all the bulk powder have been transformed into nanosheet-like spheres structure with the average diameter of about 2 μm and the thickness of about 30 nm. Compared with the diameter of nanosheet-like sphere in images (a) and (c), the diameter of nanosheet-like spheres in image (d) becomes smaller and more uniform without much change in the nanosheets thickness. This phenomenon further indicates that the final nanosheet-like sphere structure is transformed from the bulk precursor powder.

4. Discussion

By adding oxalic acid as the reductant and ammonium metavanadate as the raw material into ethanol solution, we observed the morphology transformation of V_2O_5 precursor at different reaction times. To explain the morphology transformation process of the vanadium pentoxide precursor, we attempt to illustrate the mechanism from two aspects including thermodynamics and molecular structure. During the process, we dissolved the oxalic acid in ethanol. As we know, both ethanol and oxalic acid have reducibility. The oxalic acid reducibility comes from its carboxyl group and the ethanol

reducibility comes from its hydroxyl group. Since the reducibility of oxalic acid is much stronger than the ethanol and oxalic acid is totally enough. So, in our strategy, ethanol is just the solvent and oxalic acid acts as the reductant. As a kind of organic acid, the carboxyl group can react with partial vanadium acid radical which comes from the ammonium metavanadate. The basic reaction can be formulated in Eq. (1), which in turn comprises two half reactions (Eqs. (2) and (3)) [24].

$$2VO_3^- + HCOOH + 2H^+ \rightarrow 2VO_2 + CO_2 + 2H_2O \quad (1)$$

$$VO_3^- + 2H^+ + e^- \rightarrow VO_2 + H_2O \quad E^0 = +1.00\ V \quad (2)$$

$$CO_2 + 2H^+ + 2e^- \rightarrow HCOOH \quad E^0 = -0.20\ V \quad (3)$$

On the basis of standard reduction potential (E^0) values, the standard Gibbs free energy change ΔG_m^0 of the redox reaction in Eq. (1) was estimated to be −231.6 kJ/mol, demonstrating a very strong tendency for the reaction to progress toward the products. The equation above (Eq. (1)) reveals that the reaction of carboxyl group and partial vanadium acid is radical. But in our experiments, the active groups of the reaction are carboxyl group and anionic vanadium. So, we think these equations as mentioned above also can be used to explain the mechanism of the process. In our strategy, the oxalic acid plays the role of the formic acid. Because the mole ratio of the oxalic acid to ammonium metavanadate is 10, which is much more than that in Eq. (1) so there is much enough oxalic acid in the solution. From the SEM images, we can see that in the beginning of the reaction, some stacked layers, which are marked by the yellow arrow in Fig. 2a, appear at the edge of the bulk material. Then the bulk materials begin to split to layer by layer because of the strong insertion ability of $C_2O_4^{2-}$ [25]. The insertion process keeps going with the reaction time increasing. Finally, the whole bulk material is split into layers by layers, which is shown in Fig. 2b. The $C_2O_4^{2-}$ ions are absorbed on the surface of the layers, leading surface layers to the electronegativity. In order to reduce the high surface energy of the long straight layers to achieve a more stable state system, the long straight layers bend and gather into sphere, spontaneously. Because of the electrostatic repulsive-force, the broken pieces cannot be stacked again but arranged randomly with a space of ca. 200 nm. Such a distance can balance exactly to the electrostatic repulsion and makes the system energy minimum. Then, we calcined the final products at 450 °C for 2 h and the pure vanadium pentoxide was synthesized. The schematic representation of morphology transformation processes were shown in Fig. 3.

The photocatalytic activities of precipitates obtained at different reaction times were evaluated via measuring the photodegradation of RhB under UV light irradiation (Fig. 4). The order of photocatalytic activity of catalysts is as follows: nanosheets-like spheres (S4) > nanosheet-like spheres formed on bulk (S3) > layer by layer structure (S2) > bulk material (S1). Based on the experimental observation and results, we supposed that the surface morphologies made a great contribution to photocatalytic activity. In our experiments, nanosheet-like spheres consisting of randomly packed nanosheets exhibited the highest activity, which can be further studied through multiple reflection, refraction, and diffraction inside the randomly packed nanosheets [a].

5. Conclusion

In summary, vanadium pentoxide precursor was synthesized successfully with induction of oxalic acid dissolving in ethanol

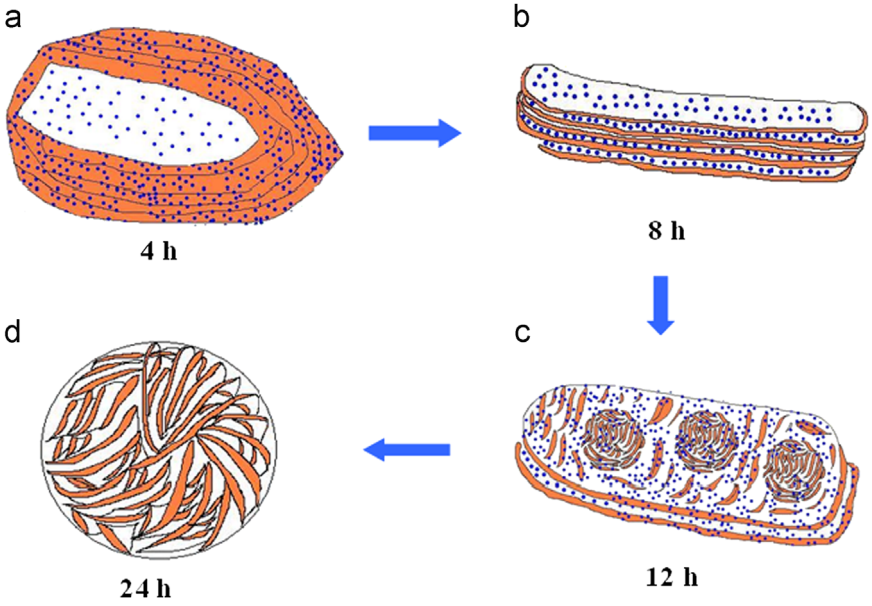

Fig. 3. Four different morphologies of vanadium pentoxide precursor schematics: (a) S1 program (suspension liquid react at 180 °C for 4 h), (b) S2 program (suspension liquid react at 180 °C for 8 h), (c) S3 program (suspension liquid react at 180°C for 12 h), (d) S4 program (suspension liquid react at 180 °C for 24 h). The blue particles in schematics are the $C_2O_4^{2-}$ ions and the orange layers are the bulk vanadium pentoxide precursor. (For interpretation of the references to color in this figure legend, the reader is referred to the web version of this article.)

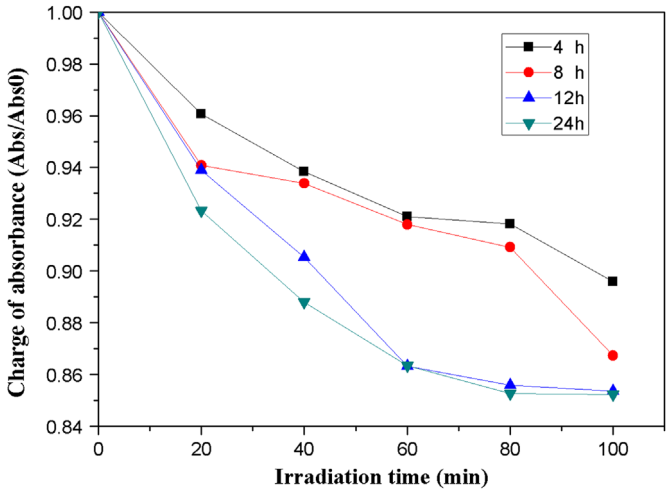

Fig. 4. Photocatalytic activities of V_2O_5 for RhB degradation: (■) precipitate obtained by reacting for 4 h, (●) precipitate obtained by reacting for 8 h, (▲) precipitate obtained by reacting for 12 h, (▼) precipitate obtained by reacting for 24 h.

solution under mild conditions. Grounded upon our experimental results, we propose that the oxalic acid and reaction time play important roles in the evolvement of vanadium pentoxide precursor crystals. When the reaction time is short, the precursor is bulk and its size is very large. With the increase of reaction time, the bulk precursor split into thin layers and finally transformed to nanosheet-like sphere structures. The nanosheet-like spheres consisting of randomly packed nanosheets exhibited the highest photocatalytic activity for degrading RhB under UV light irradiation. Based on the experimental results we have observed, the possible evolution mechanism have been discussed by employing FESEM and XRD methods and it can explain the morphology transformation process reasonably.

Acknowledgments

This work was supported by the Natural Science Foundation Project of CQ CSTC (No. 2010BB4054).

References

[1] X. Peng, L. Manna, W.D. Yang, J. Wikham, E. Scher, A. Kadavanich, A.P. Alivisatos, Shape control of CdSe nanocrystals, Nature 404 (2000) 59–61.
[2] J. Xie, Q. Wu, D. Zhang, Y. Ding, Biomolecular-induced synthesis of self-assembled hierarchical La(OH)CO_3 one-dimensional nanostructures and its morphology-held conversion toward La_2O_3 and La$(OH)_3$, Crystal Growth and Design 9 (2009) 3889–3897.
[3] J. Chen, F. Cheng, Combination of lightweight elements and nanostructured materials for batteries, Accounts of Chemical Research 42 (2009) 713–723.
[4] M.H. Huang, S. Mao, H. Feick, H.Q. Yan, Y.Y. Wu, H. Kind, E. Weber, R. Russo, P.D. Yang, Room-temperature ultraviolet nanowire nanolasers, Science 292 (2001) 1897–1899.
[5] J. Polleux, A. Gurlo, N. Barsan, U. Weimar, M. Antonietti, M. Niederberger, Template-free synthesis and assembly of single-crystalline tungsten oxide nanowires and their gas-sensing properties, Angewandte Chemie International Edition 45 (2006) 261–265.
[6] T. Xia, Q. Li, X.D. Liu, J. Meng, X.Q. Cao, Morphology-controllable synthesis and characterization of single-crystal molybdenum trioxide, Journal of Physical Chemistry B 110 (2006) 2006–2012.
[7] S. Hu, X. Wang, Single-walled MoO_3 nanotubes, Journal of the American Chemical Society 130 (2008) 8126–8127.
[8] N. Asim, S. Radiman, M.A. Yarmo, M.S. Banaye Golriz, Vanadium pentoxide: synthesis and characterization of nanorod and nanoparticle V_2O_5 using CTAB micelle solution, Microporous and Mesoporous Materials 120 (2009) 397–401.
[9] C. Wang, E. Shen, E. Wang, L. Gao, Z. Kang, C. Tian, Y. Lan, C. Zhang, Controllable synthesis of ZnO nanocrystals via a surfactant-assisted alcohol thermal process at a low temperature, Materials Letters 59 (2005) 2867–2871.
[10] L. Wang, J. Dai, X. Liu, Z. Zhu, X. Huang, P. Wu, Morphology-controlling synthesis of ZnS through a hydrothermal/solvthermal method, Ceramics International 38 (2012) 1873–1878.
[11] Ian Y.Y. Bu, Yih-Min Yeh, Effects of sulfidation on the optoelectronic properties of hydrothermally synthesized ZnO nanowires, Ceramics International 38 (2012) 3869–3873.
[12] J. Yu, H. Yu, H. Guo, M. Li, S. Mann, Spontaneous formation of a tungsten trioxide sphere-in-shell superstructure by chemically induced self-transformation, Small 4 (2008) 87–91.
[13] E.J. Jeon, Y.W. Shin, S.C. Nam, W.J. Cho, Y.S. Yoon, Characterization of all-solid-state thin-film batteries with V_2O_5 thin-film cathodes using ex situ and insitu processes, Journal of the Electrochemical Society 184 (2001) 318–322.
[14] B. Li, Y. Xu, G. Rong, M. Jing, Y. Xie, Vanadium pentoxide nanobelts and nanorolls: from controllable synthesis to investigation of their electrochemical properties and photocatalytic activities, Nanotechnology 17 (2006) 2560–2566.
[15] H.L. Fei, H.J. Zhou, J.G. Wang, P.C. Sun, D.T. Ding, T.H. Chen, Synthesis of hollow V_2O_5 microspheres and application to photocatalysis, Solid State Sciences 10 (2008) 1276–1284.
[16] F. Zhou, X. Zhao, C. Yuan, L. Li, Vanadium pentoxide nanowires: hydrothermal synthesis, formation mechanism, and phase control parameters, Crystal Growth and Design 2 (2008) 723–727.
[17] W.A. Jr, C. Ribeiro, E.R. Leite, V.R. Mastelaro, Growth kinetics of vanadium pentoxide nanostructures under hydrothermal conditions, Journal of Crystal Growth 312 (2010) 3555–3559.
[18] Ch.V. Subba Reddy, J. Wei, Z. Quan-Yao, D. Zhi-Rong, C. Wen, Sun-il Mho, Rajamohan R. Kalluru, Cathodic performance of (V_2O_5+PEG) nanobelts for Li ion rechargeable battery, Journal of Powder Sources 166 (2007) 244–249.
[19] A. Sakunthala, M.V. Reddy, S. Selvaselarapandian, B.V.R. Chowdari, P. Christopher Selvin, Energy storage studies of bare and doped vanadium pentoxide, $(V_{1.95}M_{0.05})O_5$, M=Nb, Ta, for lithium ion batteries, Energy and Environmental Science 4 (2011) 1712–1725.
[20] C.Q. Feng, S.Y. Wang, R. Zeng, Z.P. Guo, K. Konstantinov, H.K. Liu, Synthesis of spherical porous vanadium pentoxide and its electrochemical properties, Journal of Power Sources 184 (2008) 485–488.
[21] Y. Chen, H. Liu, W.L. Ye, Preparation and electrochemical properties of submicron spherical V_2O_5 as cathode material for lithium ion batteries, Scripta Materialia 59 (2008) 372–375.
[22] H.L. Fei, H.J. Zhou, J.G. Wang, P.C. Sun, D.T. Ding, T.H. Chen, Synthesis of hollow V_2O_5 microspheres and application to photocatalysis, Solid State Sciences 10 (2008) 1276–1284.
[23] H.L. Fei, H.J. Zhou, J.G. Wang, P.C. Sun, D.T. Ding, T.H. Chen, Synthesis of V_2O_5 micro-architectures via in situ generation of single-crystalline nanoparticles, Solid State Sciences 11 (2009) 102–107.
[24] J. Liu, Q. Li, T. Wang, D. Yu, Y. Li, Metastable vanadium dioxide nanobelts: hydrothermal synthesis, electrical transport, and magnetic properties, Chemie International Edition 43 (2004) 5048–5052.
[25] L. Li, J. Zhao, Y. Wang, Y. Li, D. Ma, Y. Zhao, S. Huo, X. Hao, Oxalic acid mediated synthesis of $WO_3 \cdot H_2O$ nanoplates and self-assembled nanoflowers under mild conditions, Journal of Solid State Chemistry 184 (2011) 1661–1665.